Chinese Chemical Letters 37 (2026) 112063

Contents lists available at ScienceDirect

Chinese Chemical Letters

journal homepage: www.elsevier.com/locate/cclet

Discovery of 2-oxopiperazine derivatives as novel GPX4 inhibitors for the treatment of oral cancer

Anxiang Yang[a,1], Sunkai Gu[a,1], Ziyi Jiao[a,1], Yuhao Feng[a], Hui Sun[a], Guanyu Yang[a], Minghui Gao[a], Tao Zeng[a], Benxin Hou[b], Ling Huang[a,*], Xiaokun Wang[a,*], Congjun Xu[a,*], Haibin Luo[a]

[a] Key Laboratory of Tropical Biological Resources of Ministry of Education, School of Pharmaceutical Sciences, Hainan University, Haikou 570228, China
[b] Department of General Surgery, Sanya Central Hospital (Hainan Third People's Hospital), Sanya 572000, China

ARTICLE INFO

Article history:
Received 23 September 2025
Revised 3 November 2025
Accepted 4 November 2025
Available online 5 November 2025

Keywords:
GPX4 inhibitor
Ferroptosis
Hybridization
Oral cancer
Selective

ABSTRACT

Inducing ferroptosis is a promising strategy for oral cancer therapy, but existing inducers often lack selectivity and possess poor drug-like properties. Our preliminary work identified **26a** as a potent ferroptosis inducer targeting glutathione peroxidase 4 (GPX4), yet its selectivity and safety needed improvement. In this study, we designed a series of hybrid molecules by integrating the privileged fragment of **26a** with the known GPX4 inhibitor ML210. Subsequent structural modifications led to the discovery of XW19, a novel structural scaffold exhibiting GPX4 inhibitory activity. XW19 demonstrated enhanced ferroptosis-inducing potency and highly selectivity (selectivity index (SI) = 1200) as well as inhibitory effects against oral cancer (half maximal inhibitory concentration (IC_{50}) values ranging from 0.71 μmol/L to 2.39 μmol/L). Cellular thermal shift assay (CETSA) confirmed the strong binding affinity of XW19 with GPX4. Notably, XW19 exhibited significant tumor suppression and an improved safety profile in a nude mouse model bearing Cal27 ectopic xenografts, positioning XW19 as a promising therapeutic candidate for oral cancer treatment.

© 2026 Published by Elsevier B.V. on behalf of Chinese Chemical Society and Institute of Materia Medica, Chinese Academy of Medical Sciences.

Oral cancer (OC) is an aggressive malignant neoplasm originating from the oral cavity and its associated anatomical structures, including the gingiva, oropharynx, tongue, lips, and palate [1–3]. Global epidemiological data from 2022 indicates that oral cancer accounted for approximately 390,000 newly diagnosed cases and 200,000 mortality-related outcomes worldwide [4]. Oral cancer exhibits notable geographic disparities, with escalating incidence rates observed in Southeast Asia and specific Chinese regions including Hainan and Taiwan provinces [5]. Contemporary chemotherapeutic regimens, though clinically indispensable, show suboptimal response rates (~50%), highlighting critical gaps in targeted molecular interventions [6].

Ferroptosis, a newly characterized form of regulated cell death driven by iron-dependent accumulation of lipid peroxides, has emerged as a promising therapeutic strategy [7], particularly for refractory oral cancers [8]. Moreover, induction of ferroptosis has also shown potential in reversing resistance to chemotherapy [9] and radiotherapy, thereby maximizing clinical therapeutic efficacy [10].

The cystine/glutamate antitransporter (xCT)-glutathione/glutathione peroxidase 4 (GPX4) axis serves as the central regulatory machinery governing cellular defense against ferroptosis, with coordinated cystine uptake and lipid peroxide reduction constituting its core mechanistic framework. The xCT inhibitor erastin significantly induced ferroptosis in HSC-2 and SAS oral squamous cell carcinoma (OSCC) cell lines, particularly in those exhibiting an epithelial-mesenchymal transition (EMT)-driven mesenchymal phenotype, which appears more susceptible to ferroptotic cell death. Similarly, RSL3, a GPX4 inhibitor, enhances the efficacy of radiation therapy in OSCC cells in mouse xenograft models, providing a mechanistic rationale for ferroptosis-targeted therapies in aggressive OSCC subtypes [8,11].

In our previous work, a more selective ferroptosis inducer compound **26a** targeting GPX4 was discovered, and **26a** demonstrated excellent anti-proliferative activity on a variety of tumor cell lines [12,13]. However, **26a** exhibits poor water solubility and exhibits certain toxic effects. Its chloroacetyl moiety, acting as an electrophilic warhead, is the primary cause of its unfavorable pharmacokinetic and pharmacodynamic profiles. ML210 is regarded as a

* Corresponding authors.
E-mail addresses: linghuang@hainanu.edu.cn (L. Huang), wangxk@hainanu.edu.cn (X. Wang), congjunxu@hainanu.edu.cn (C. Xu).
[1] These authors contributed equally to this work.

https://doi.org/10.1016/j.cclet.2025.112063
1001-8417/© 2026 Published by Elsevier B.V. on behalf of Chinese Chemical Society and Institute of Materia Medica, Chinese Academy of Medical Sciences.

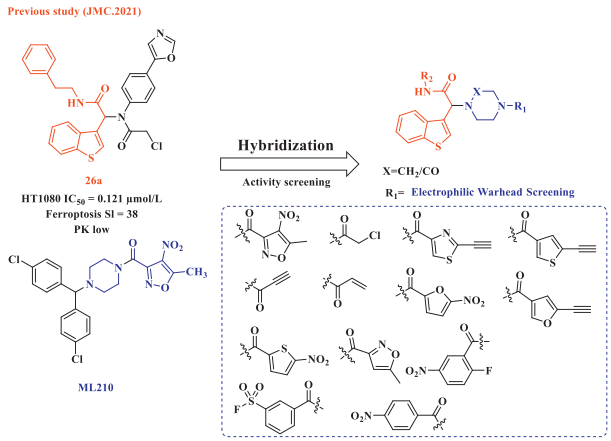
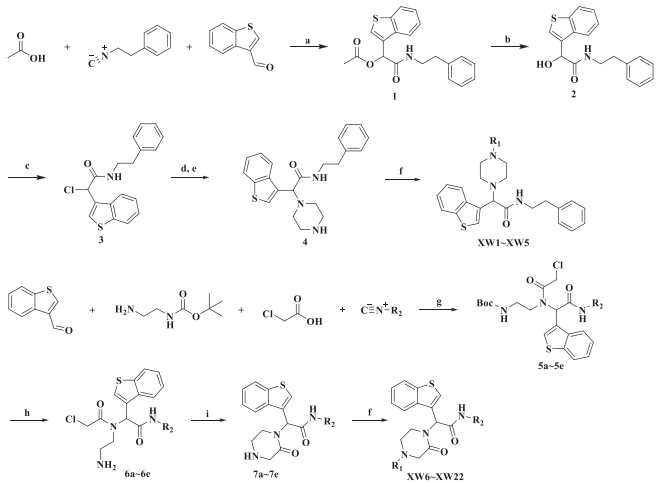


Fig. 1. Design strategies for the novel GPX4 inhibitors.

classic GPX4 inhibitor, and combining its piperazine moiety with novel electrophilic fragments offers significant potential for addressing the issues [14].

In this study, structure-based molecular hybridization was used to strategically integrate the privileged benzothiophene acetamide scaffold of **26a** with the piperazine pharmacophore from ML210. Building upon this molecular framework, we systematically explored structure-activity relationships (SAR) through strategic incorporation of diverse electrophilic warheads (Fig. 1). Optimized compound XW19 demonstrates potent ferroptosis-inducing activity with remarkable selectivity (selectivity index (SI) = 1200) and enhanced aqueous solubility. This novel agent exhibits strong growth suppression against multiple oral cancer cell lines, and thermal shift assays validate its direct engagement with the GPX4 protein target. Notably, *in vivo* evaluations reveal significant tumor growth inhibition in oral cancer xenograft models coupled with an excellent safety profile, positioning XW19 as a promising therapeutic candidate for oral cancer treatment.

The synthetic routes for targeted compounds were strategically developed through multicomponent reaction-driven divergent synthesis (Scheme 1). The synthesis of XW1–XW5 begins with the Passerini reaction, generating the key benzothiophene acetamide intermediate **1**. Following sequential hydrolysis, chlorination, nucleophilic substitution, and acylation transformations, the intermediate was elaborated into the final A-series compounds. In parallel, XW6–XW22 was synthesized through a four-component Ugi protocol, yielding chloroacetamide intermediates **5a**–**5e**. These intermediates underwent Boc deprotection, followed by nucleophilic cyclization to establish the core scaffold, and were subsequently subjected to late-stage acylation to afford the target compounds XW6–XW22.

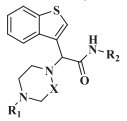


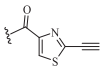
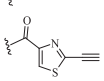
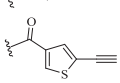
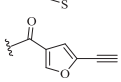
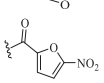
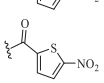
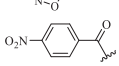
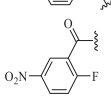
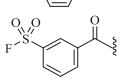
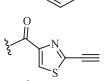
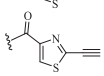
Scheme 1. Synthesis of compounds XW1–XW22. Reagents and conditions: (a) DCM, r.t., 12 h; (b) MeOH, H_2O, LiOH, r.t., 6 h; (c) $SOCl_2$, DCM, r.t., 10 h; (d) *tert*–butyl piperazine-1-carboxylate, MeCN, 90 °C, N_2, 10 h; (e) TFA, DCM, r.t., 6 h; (f) carboxylic Acid, EDCI, HOBT, triethylamine, DMF, 10 h; (g) MeOH, r.t., 12 h; (h) TFA, DCM, r.t., 6 h; (i) $CsCO_3$, DMF, 90 °C, 10 h.

Our initial investigation focused on two molecular hybrid compounds (XW1 and XW2) containing chloracetyl and 5-methyl-4-nitroisoxazole-3-carbonyl as distinct electrophilic warheads, respectively. As shown in Table 1, cytotoxicity profiling revealed that compound **26a** exhibited moderate antiproliferative activity against CAL27, SCC-25, and WSU-HN30 oral cancer cells (half maximal inhibitory concentration (IC_{50}) = 2.85–13.68 μmol/L), but showed minimal effect on SAS cells (IC_{50} > 20 μmol/L). In contrast, ML210 demonstrated potent cytotoxicity in fibrosarcoma HT1080 cells with high ferroptosis selectivity (confirmed by inhibitor rescue assays), yet was inactive against all four oral cancer cell lines (IC_{50} > 20 μmol/L). XW1 exhibited neither significant cytotoxicity nor ferroptosis selectivity, while XW2 demonstrated promising oral cancer inhibitory activity. This marked contrast in biological outcomes highlights the critical influence of electrophilic warhead selection on pharmacological profiles within this structural class. Guided by these findings, we subsequently designed compounds XW3–XW5 through the replacement of the electrophilic warheads. Furthermore, to investigate the impact of heterocyclic modifications on bioactivity, we implemented an isosteric replacement strategy by substituting the CH_2 group in the piperazine ring with a carbonyl group (CO), leading to the synthesis of analogs XW6–XW10. Lactam ring-containing analogs exhibited enhanced anti-oral cancer activity. For instance, compound XW8 demonstrated superior potency with IC_{50} values of 1.61 μmol/L (Cal27), 3.09 μmol/L (SCC25), 0.91 μmol/L (WSU-HN30), and 4.78 μmol/L (SAS), representing an improvement compared to the parent compound XW3 across all tested cell lines, underscoring the pharmacophoric advantage of the lactam. This SAR-driven discovery prompted systematic exploration of electrophilic warheads (XW11–XW19) [8,15–20] to evaluate their ability to induce ferroptosis and inhibit oral cancer cell proliferation. The results revealed that electrophilic fragments such as 5-formylthiophene-3-carbonyl, 5-formylfuran-3-carbonyl, and 5-nitrofuran-2-carbonyl conferred certain ferroptosis-inducing activity and anti-oral cancer effects. In contrast, fragments such as 5-nitrothiophene-2-carbonyl (compounds XW14–XW18) resulted in a complete loss of activity. These findings suggest that GPX4 inhibitors exhibit a degree of conservativity regarding the electrophilic moiety. Among the evaluated warheads, 2-ethynylthiazole-4-carboxamide (XW19) emerged as the most favorable, conferring marked ferroptosis selectivity (SI = 1201) and potent antiproliferative activity against oral cancer cell lines (IC_{50} = 0.71–2.39 μmol/L). Finally, the effects of distinct amides on biological activity were investigated. Compounds bearing benzyl (XW19), tert–butyl (XW20), 4-fluorophenethyl (XW21), or cyclohexyl (XW22) substituted amides all retained good potency, and the benzyl-containing compound XW19 exhibited enhanced inhibitory activity against oral cancer cells with ferroptosis selectivity. Consequently, XW19 was selected as the lead compound for further investigation.

To validate the protein targets of the compounds, extracellular GPX4 inhibitory activity was assessed (Fig. S1 in Supporting information). The results indicated that both XW19 and **26a** exhibited significant inhibitory activity against GPX4. In contrast, ML210 did not show any extracellular GPX4 inhibition, as it is a prodrug that requires intracellular biotransformation to bind GPX4 [21]. Following compound treatment, a decrease in intracellular GPXs activ-

Table 1
Ferroptosis selectivity and cytotoxicity against HT1080 cells and oral cancer cell lines including Cal27, SCC25, WSU-HN30, and SAS of **26a**, ML210 and XW1–XW22.



Entry	R_1	R_2	X	IC_{50} ± SD (μmol/L)						
				HT1080	HT1080[a]	SI[b]	Cal27	SCC25	WSU-HN30	SAS
26a	-	-	-	0.121 ± 0.039	4.60 ± 0.04	38[c]	2.85 ± 0.44	12.16 ± 1.84	13.68 ± 3.99	>20
ML210	-	-	-	0.32 ± 0.09	>100	>312	>20	>20	>20	>20
XW1			CH_2	>10	NT[d]	NT	>20	>20	>20	>20
XW2			CH_2	10.00 ± 0.04	20.80 ± 8.10	2	8.29 ± 0.72	6.49 ± 0.06	11.53 ± 3.34	2.38 ± 1.43
XW3			CH_2	0.75 ± 0.04	21.92 ± 0.72	29	1.81 ± 0.68	5.10 ± 0.01	4.33 ± 0.07	3.13 ± 2.08
XW4			CH_2	3.11 ± 0.53	17.73 ± 3.17	5	1.75 ± 0.42	2.17 ± 1.65	6.27 ± 3.68	3.97 ± 0.11
XW5			CH_2	>10	NT	NT	>20	>20	>20	>20
XW6			CO	>10	NT	NT	>20	>20	>20	>20
XW7			CO	1.313 ± 0.681	12.98 ± 0.80	10	1.85 ± 1.02	3.16 ± 0.34	2.12 ± 0.18	2.09 ± 0.73
XW8			CO	0.005 ± 0.003	12.60 ± 0.79	2521	1.61 ± 0.16	3.09 ± 1.15	0.91 ± 0.31	4.78 ± 1.11
XW9			CO	0.372 ± 0.037	17.47 ± 0.74	47	5.46 ± 0.29	9.50 ± 3.40	5.70 ± 1.08	8.76 ± 2.79
XW10			CO	>10	NT	NT	>20	>20	>20	>20
XW11			CO	0.480 ± 0.022	>40	83	10.67 ± 0.69	11.40 ± 3.36	7.66 ± 1.62	>20
XW12			CO	0.481 ± 0.030	>40	83	8.07 ± 0.53	8.87 ± 2.95	6.46 ± 1.55	>20
XW13			CO	7.562 ± 0.063	NT	NT	4.13 ± 0.81	6.33 ± 2.72	5.90 ± 1.30	4.91 ± 1.33
XW14			CO	>10	NT	NT	>20	>20	>20	>20
XW15			CO	>10	NT	NT	11.38 ± 0.78	>20	14.76 ± 3.37	9.84 ± 3.83
XW16			CO	>10	NT	NT	>20	>20	>20	>20
XW17			CO	>10	NT	NT	>20	>20	>20	>20
XW18			CO	>10	NT	NT	>20	>20	>20	>20
XW19			CO	0.014 ± 0.049	16.81 ± 0.58	1201	0.80 ± 0.06	1.89 ± 1.04	0.71 ± 0.19	2.39 ± 0.23
XW20			CO	0.023 ± 0.008	14.26 ± 0.54	620	2.30 ± 0.22	3.65 ± 0.54	1.23 ± 0.51	5.13 ± 3.37
XW21			CO	0.008 ± 0.005	1.88 ± 0.38	235	1.05 ± 0.16	2.40 ± 1.24	1.43 ± 1.10	5.60 ± 1.90
XW22			CO	0.035 ± 0.014	16.11 ± 0.51	460	3.85 ± 1.67	4.78 ± 4.41	2.01 ± 0.63	6.73 ± 3.79

[a]HT1080 incubated with compounds and Fer-1 0.5 μmol/L.
[b]HT1080[a] IC_{50}/HT1080 IC_{50}.
[c]The results are consistent with those of previous studies.
[d]No tested.

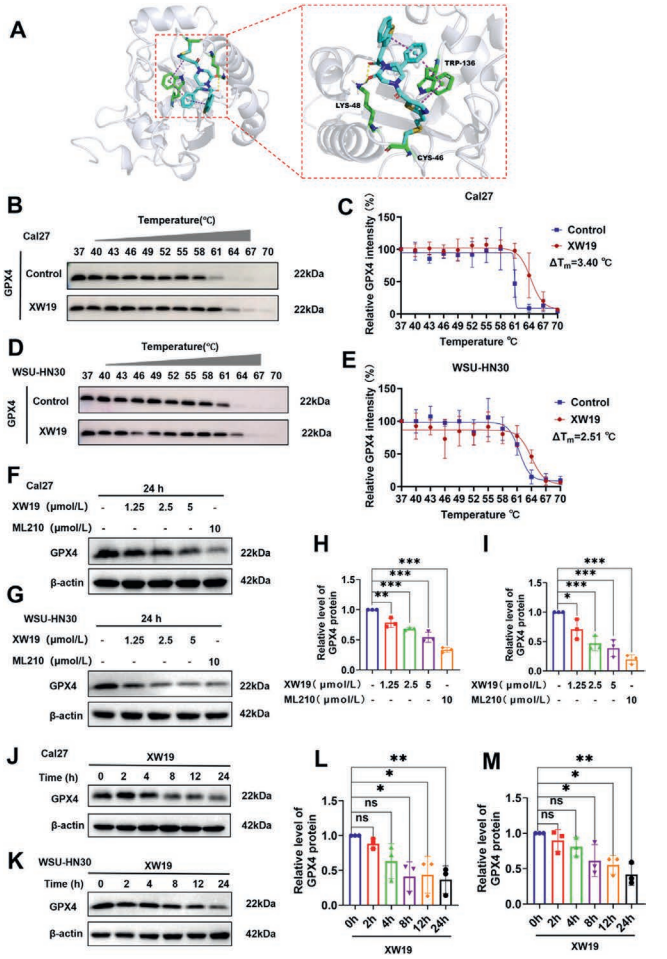


Fig. 2. XW19 facilitates the degradation of GPX4 through direct binding. (A) Molecular docking model of XW19 bound to GPX4 (PDB ID: 6HKQ). (B–E) CETSA temperature gradient profiles and quantification demonstrating XW19-GPX4 interaction in Cal27 and WSU-HN30 cells. (F–I) XW19 downregulated GPX4 protein expression in a concentration-dependent manner. (J–M) XW19 decreased the protein expression of GPX4 in a time-dependent manner. Data are presented as mean ± standard deviation (SD) ($n = 3$). $^{*}P < 0.05$, $^{**}P < 0.01$, $^{***}P < 0.001$. n.s, no significance.

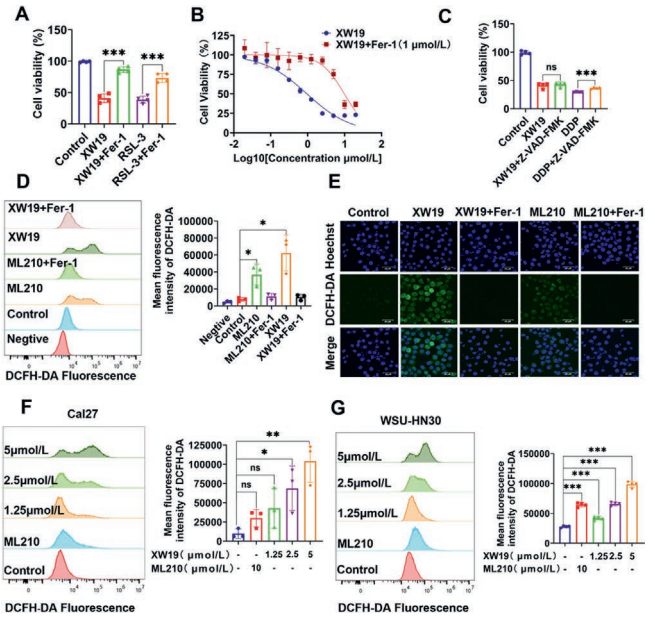


Fig. 3. XW19 induces ferroptosis in oral cancer cells *via* reactive oxygen species (ROS) accumulation. (A) Viability of Cal27 cells treated with XW19 (2.5 μmol/L) was rescued by the Fer-1 ($n = 4$). (B) Cytotoxicity of XW19 with or without co-treatment with Fer-1 ($n = 3$). (C) The apoptosis inhibitor Z-VAD-FMK did not alleviate XW19-induced cytotoxicity. DDP: *cis*-diamminedichloroplatinum, an apoptosis inducer ($n = 4$). (D) Intracellular ROS levels were measured using the fluorescence probe DCFH-DA by flow cytometry. XW19 and ML210 increased ROS accumulation, which was reversed by Fer-1 ($n = 3$). (E) Representative images of intracellular ROS were obtained by confocal fluorescence microscopy. Nuclei were stained with Hoechst 33342. Scale bar: 40 μm. (F, G) XW19 induced ROS generation in a concentration-dependent manner in Cal27 and WSU-HN30 cells ($n = 4$). Data are presented as mean ± SD. $^{*}P < 0.05$, $^{**}P < 0.01$, $^{***}P < 0.001$.

ity was also observed. These results collectively demonstrate that XW19 possesses remarkable GPX4 inhibitory activity. To elucidate the molecular recognition mode of XW19 with GPX4, molecular docking studies were performed. As depicted in Fig. 2A, the alkyne group on the thiazole ring forms a critical covalent bond with CYS-46, consistent with previous reports. Additionally, a network of π-π interactions involving the thiazole, benzyl ring, and benzothiophene moieties with residue TRP-136 stabilizes the compound conformation. Notably, hydrogen bonds form between the oxygen atoms of the two amide bonds and residue LYS-48. Collectively, these interactions underpin the strong binding affinity of compound XW19 for GPX4, accounting for its potent GPX4 inhibitory activity and consequent antitumor effects. To further validate the target engagement, the cellular thermal shift assay (CETSA) [22] was performed in Cal27 and WSU-HN30 cell lines. As shown in Figs. 2B–E, incubation with XW19 increased the thermal stability of GPX4, resulting in thermal shifts (ΔT_m) of 3.40 and 2.51 °C, respectively. These findings demonstrate that XW19 effectively binds to GPX4 in a cellular context. Furthermore, treatment with XW19 resulted in both dose- (Figs. 2F–I) and time- (Figs. 2J–M) dependent depletion of cellular GPX4 protein levels. However, XW19 treatment did not affect GPX4 mRNA expression (Fig. S2A in Supporting information), suggesting that compound binding may facilitate GPX4 protein degradation. Consistently, MG132, a proteasome inhibitor, blocked XW19-induced GPX4 degradation, whereas leupeptin had no effect (Figs. S2B–E in Supporting information). Collectively, these results indicate that XW19 binds to GPX4 and promotes its proteasome-mediated degradation.

The ferroptosis selectivity of XW19 was evaluated in oral cancer CAL27 cells. As shown in Figs. 3A and B, the cytotoxicity of XW19 was significantly reversed by the ferroptosis inhibitor ferrostatin-1 (Fer-1), whereas the apoptosis inhibitor Z-VAD-FMK, the necroptosis inhibitor necrostatin-1 (Nec-1), and the autophagy inhibitor 3-MA did not attenuate XW19-induced cytotoxicity (Fig. 3C, Figs. S3A and B in supporting information). Moreover, XW19 exhibited lower cytotoxicity toward normal cells compared with **26a**, with IC_{50} values of 11.55 ± 0.48 μmol/L in mouse fibroblasts L929 and 13.65 ± 1.05 μmol/L in human oral keratinocytes HOK. In contrast, **26a** displayed IC_{50} values of 7.00 ± 0.48 and 8.21 ± 0.36 μmol/L in L929 and HOK cells, respectively (Figs. S3C and D in Supporting information). These results demonstrate that XW19 selectively induces ferroptosis in oral cancer cells. Consistently, both flow cytometry and confocal microscopy analyses (Figs. 3D and E) [23] demonstrated that XW19 significantly increased the levels of oxidative stress, which were reversed by Fer-1. Importantly, the elevation of oxidative stress and lipid peroxidation exhibited a concentration-dependent pattern in Cal27 and WSU-HN30 cell lines following XW19 treatment (Figs. 3F and G, Figs. 4A and B). Additionally, XW19 increased the labile iron pool (LIP) in both cell lines (Figs. 4C and D), thereby amplifies lipid peroxidation and establishing a self-reinforcing cycle that drives ferroptotic cell death. Morphological evidence of ferroptosis was further confirmed by the presence of characteristic mitochondrial alterations, including

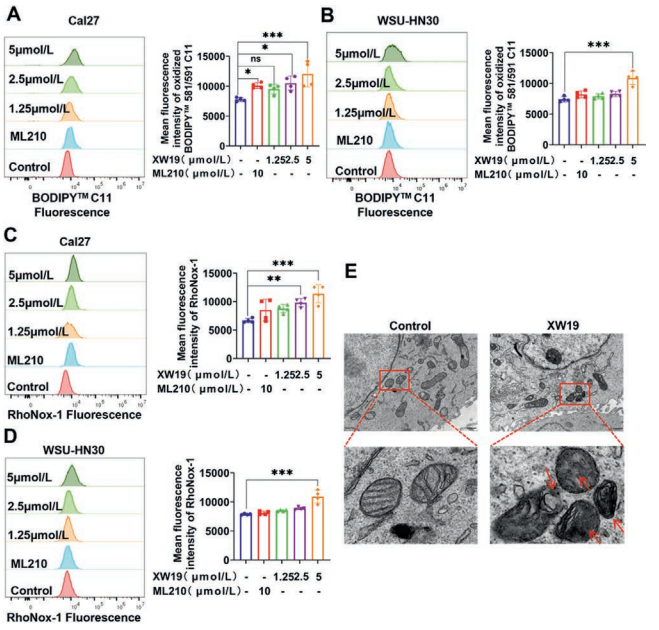


Fig. 4. XW19 triggers ferroptosis *via* lipid peroxidation, iron accumulation, and mitochondrial damage. Flow cytometry analysis of BODIPY^{TM} 581/591 C11-stained Cal27 (A) and WSU-HN30 (B) cells showing a dose-dependent increase in lipid peroxidation following XW19 treatment. (C, D) Intracellular Fe^{2+} levels were assessed by flow cytometry using the RhoNox-1 fluorescent probe. XW19 treatment led to increased iron accumulation. (E) Transmission electron microscopy images revealed XW19 treatment altered the mitochondria morphology. Red arrow: mitochondria membrane damage, shrinkage and loss of mitochondrial cristae. Scale bar: 500 nm. Data are presented as mean ± SD ($n = 4$). $^{*}P < 0.05$, $^{**}P < 0.01$, $^{***}P < 0.001$.

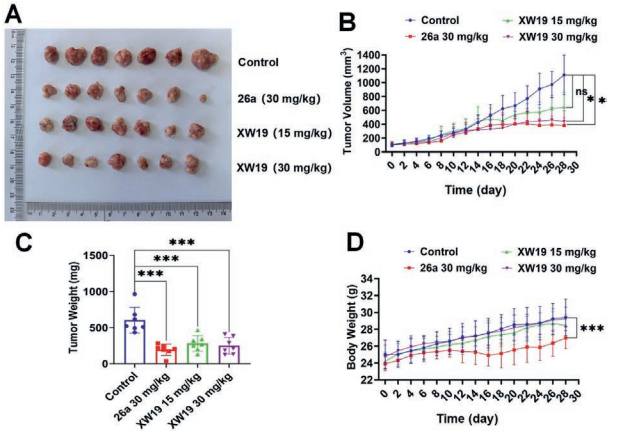


Fig. 5. XW19 inhibits tumor growth without causing systemic toxicity in xenograft models. Treatment with XW19 or **26a** significantly reduced tumor volume (A, B) and tumor weight (C) in Cal27-derived xenograft models ($n = 7$ per group). (D) XW19 had no significant effect on body weight, whereas **26a** treatment led to a marked decrease. Data are presented as mean ± SD. $^{*}P < 0.05$, $^{***}P < 0.001$.

shrinkage and loss of cristae, observed in XW19-treated cells (Fig. 4E).

Given the potent ferroptosis-inducing and anti-oral cancer activity of XW19, we further evaluated its aqueous solubility and metabolic stability. The results showed that XW19 exhibits improved solubility (3.6 μg/mL) and a plasma half-life of 119.6 min. Its *in vivo* efficacy was assessed using xenograft models. All animal experiments were approved by the Ethics Committee of Hainan University (approval No HPIACUC2024150). As shown in Fig. 5, both compound **26a** (30 mg/kg) and XW19 moderately inhibited tumor growth in Cal27-derived xenograft model, each achieving a

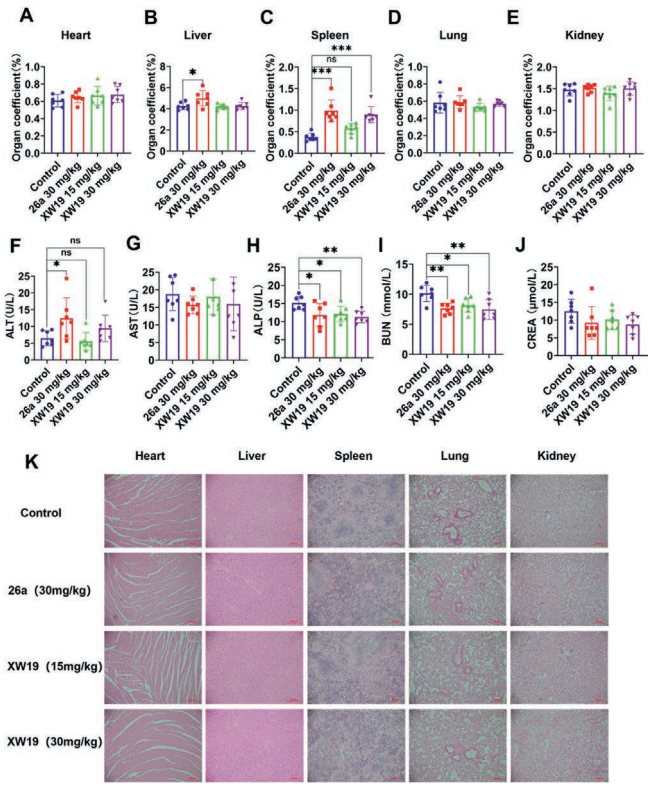


Fig. 6. Comprehensive safety evaluation of XW19 *in vivo*. (A–E) Main organ coefficient ($n = 7$ per group). Organ coefficient = (organ weight/body weight) × 100 %. Serum biochemical indices, including ALT (F), aspartate aminotransferase (AST) (G), ALP (H), blood urea nitrogen (BUN) (I) and creatinine (CREA) (J) were measured to evaluate hepatic and renal function ($n = 7$). (K) Representative hematoxylin and eosin (H&E) staining of main organs, including the heart, liver, spleen, lung and kidney. Scale bar: 200 μm. Data were presented as the mean ± SD. $^{*}P < 0.05$, $^{**}P < 0.01$, $^{***}P < 0.001$.

tumor growth inhibition (TGI) rate of 59 %, with significantly reduced tumor weights compared to control group ($P < 0.001$). However, treatment with **26a** resulted in >10 % body weight loss, indicative of systemic toxicity. A comprehensive safety assessment (Fig. 6) further revealed hepatocellular injury in the **26a**-treated group, as evidenced by increased organ coefficients (liver: +16 %; spleen: +146 %) and altered serum biochemical parameters (alanine aminotransferase (ALT): +91.8 %; alkaline phosphatase (ALP): −22 %). In contrast, XW19 did not induce significant hepatocellular injury and may exert a regulatory effect of hepatic metabolism without reaching a toxic threshold, indicating an overall favorable safety profile.

In summary, we developed a series of hybrid molecules by integrating the privileged scaffold of **26a** and ML210. Following systematic structural optimization, the lead compound XW19 was identified. XW19 exhibits remarkable ferroptosis selectivity (SI = 1200) and potent inhibitory activity against oral cancer cell lines with IC_{50} values ranging from 0.71 μmol/L to 2.39 μmol/L in Cal27, SCC25, WSU-HN30, and SAS cells. Molecular docking and CETSA in both Cal27 and WSU-HN30 cells confirmed its strong binding affinity for GPX4. Furthermore, XW19 significantly induced lipid peroxide accumulation in oral cancer cells, an effect that was reversed by ferroptosis inhibitors. Treatment with XW19 also increased intracellular ferrous iron (Fe^{2+}) levels and induced characteristic ferroptotic mitochondrial morphology. Crucially, in a Cal27 ectopic xenograft model, XW19 demonstrated significant tumor growth inhibition (TGI = 59 %) and exhibited an improved safety profile compared to **26a**. This study may provide ideas for the application of ferroptosis inducers in the treatment of oral cancer.

CRediT authorship contribution statement

Anxiang Yang: Writing – original draft, Investigation, Formal analysis, Data curation. **Sunkai Gu:** Writing – original draft, Investigation, Formal analysis, Data curation. **Ziyi Jiao:** Investigation, Formal analysis, Data curation. **Yuhao Feng:** Formal analysis, Data curation. **Hui Sun:** Software, Methodology. **Guanyu Yang:** Validation, Data curation. **Minghui Gao:** Formal analysis, Data curation. **Tao Zeng:** Visualization, Software. **Benxin Hou:** Resources, Funding acquisition. **Ling Huang:** Writing – review & editing, Supervision, Resources. **Xiaokun Wang:** Writing – review & editing, Writing – original draft, Methodology. **Congjun Xu:** Writing – review & editing, Writing – original draft, Funding acquisition, Conceptualization. **Haibin Luo:** Visualization, Project administration.

Declaration of competing interest

The authors declare that they have no known competing financial interests or personal relationships that could have appeared to influence the work reported in this paper.

Acknowledgments

This study was supported by the National Natural Science Foundation of China (Nos. 82204193, 82460119), Hainan Provincial Natural Science Foundation of China (No. 325RC657), Sanya Central Hospital Natural Science Foundation (No. SYZXYY202505), Fundamental Research Funds for Hainan University (Nos. KYQD(ZR)23146, KYQD(ZR)22007), Excellent Talent Team Project in Hainan Province (No. HNYT20250004).

Supplementary materials

Supplementary material associated with this article can be found, in the online version, at doi:10.1016/j.cclet.2025.112063.

References

[1] J.M. Wu, H. Chen, Y.J. Liu, R.T. Yang, N. An, J. Cancer Res. Clin. Oncol. 151 (2025) 53.
[2] Q. Wei, L. Chen, W. Luo, et al., Eur. J. Pharmacol. 967 (2024) 176353.
[3] Y. Liu, L. Wang, Y. Zhu, L. Lan, D. Wang, Innovat. Med. 1 (2023) 100011.
[4] GBD 2021 oral disorders collaborators, Lancet 405 (2025) 897–910.
[5] X.Y. Zhang, W.H. Xie, H. Ye, et al., BMC Oral Health 24 (2024) 938.
[6] M. Zheng, Innovat. Med. 1 (2023) 100039.
[7] A.T. Kao, C.V. Cabanlong, K. Padilla, X. Xue, Acta Pharm. Sin. B 14 (2024) 3785–3801.
[8] A. Elhami, S. Ghasemzadeh, S. Emrahoglu, et al., Naunyn Schm. Arch. Pharmacol. 398 (2025) 12847–12867.
[9] L. Li, B. Sun, J. Sun, et al., Chin. Chem. Lett. 35 (2024) 109538.
[10] J. Zhu, Q. Tan, S. Fan, et al., Chin. Chem. Lett. 37 (2026) 111285.
[11] V. Vijayarangam, M.K.G. Deviparasakthi, P. Balasubramanian, et al., Pathol. Res. Pract. 263 (2024) 155637.
[12] S.K. Gu, G.Y. Yang, H.Y. Bian, et al., J. Med. Chem. 68 (2025) 3309–3323.
[13] C. Xu, Z. Xiao, J. Wang, et al., J. Med. Chem. 64 (2021) 13312–13326.
[14] M. Weiwer, J.A. Bittker, T.A. Lewis, et al., Med. Chem. Lett. 22 (2012) 1822–1826.
[15] W. Li, J. Yu, J. Wang, et al., Chem. Sci. 15 (2024) 10477–10490.
[16] E. Karaj, S.H. Sindi, N. Kuganesan, et al., J. Med. Chem. 65 (2022) 11788–11817.
[17] T. Chen, J. Leng, J. Tan, et al., J. Med. Chem. 66 (2023) 10036–10059.
[18] S.M. Haag, M.F. Gulen, L. Reymond, et al., Nature 559 (2018) 269–273.
[19] Z.F. Tang, J. Li, L.J. Peng, et al., J. Med. Chem. 67 (2024) 1872–1887.
[20] J. Wang, Z. Deng, X. Li, et al., J. Med. Chem. 68 (2025) 15828–15848.
[21] J.K. Eaton, L. Furst, R.A. Ruberto, et al., Nat. Chem. Biol. 16 (2020) 497–506.
[22] Y. Rao, R. Su, C. Wu, X. Chai, et al., Acta Pharm. Sin. B 14 (2024) 304–318.
[23] P. Shang, J. Yang, L. Shao, et al., Pharm. Sci. Adv. 2 (2024) 100057.